STM JOURNALS

Journal of
Polymer & Composites

ISSN: 2321-2810 (Online)
ISSN: 2321-8525 (Print)
Volume 13, Issue 3, 2025
DOI (Journal): 10.37591/JoPC

https://journals.stmjournals.com/jopc

Research JoPC

Au@Sio$_2$@PVP-DCMD Membranes: A Breakthrough in Heavy Metal Removal and Antibacterial Defense

Sufyana Idrees[1], Aneeqa Sabah[2,*], Mohsin Nazir[3], Whied ul Hussan Shahzad[4], Aneela Sabbir[5], Sahar Tasleem[6]

Abstract

This study investigates the development and characterization of multifunctional gold-doped silica (Au@SiO₂) membranes for water distillation and antibacterial applications. The manufacturing process integrated gold nanoparticles into silica matrices using sol-gel techniques. Structural analysis was conducted using SEM (showing uniform pore distribution with an average pore size of 40-50 nm), FTIR (confirming Si-O-Si and Si-Au-Si bonding peaks at 525 cm^{-1} and 1310 cm^{-1} respectively), EDX (revealing gold nanoparticle content of 1.5 wt%), and UV-Visible spectroscopy (indicating an optical band gap decrease from 2.6 eV to 1.8 eV). Permeation tests demonstrated a water vapor transport rate of 3.2 kg/m²h, with heavy metal rejection rates exceeding 99.5% for Pb^{2+} and Cd^{2+}. Antibacterial efficacy was validated through microbial assays, showing a reduction of bacterial colonies by 98% for K. pneumoniae and 96% for S. aureus. Density functional theory (DFT) calculations showed that doping with gold led to a 1.2 eV reduction in the band gap, a 15% decrease in total stress, increases in elastic modulus and thermal conductivity, a 20% rise in bond energy, and an 18% increase in potential energy. The large ionic radius of gold prevented its incorporation into the silica matrix, as supported by experimental data. These results highlight the potential of (Au@SiO₂) membranes in achieving energy-efficient water distillation and effective antibacterial performance, marking a significant advancement in water purification technology.

Keywords: Au@SiO₂ membranes, saline water separation, heavy metal rejection, material studio (DFT), pathogenic bacteria

***Author for Correspondence**
Aneeqa Sabah

[1]PhD Scholar, Department of Physics, Lahore College for Women University, Lahore, Pakistan
[2]Associate Professor, Department of Physics, Lahore College for Women University, Lahore, Pakistan
[3]Chairperson, Department of Software Engineering, Lahore College for Women University, Lahore, Pakistan
[4]PhD Scholar, Department of Industrial biotechnology, Government College University, Lahore, Pakistan
[5]Associate Professor, Department of Polymer Engineering, Punjab University, Lahore, Pakistan
[6]PhD Scholar, Department of Physics, Lahore College for Women University, Lahore, Pakistan

Received Date: January 20, 2025
Accepted Date: February 08, 2025
Published Date: March 30, 2025

Citation: Sufyana Idrees, Aneeqa Sabah, Mohsin Nazir, Whiedul Hussan Shahzad, Aneela Sabbir, Sahar Tasleem. Au@SiO$_2$@PVP-DCMD Membranes: A Breakthrough in Heavy Metal Removal and Antibacterial Defense. Journal of Polymer & Composites. 2025; 13(3): 13–27p.

INTRODUCTION

Various water and wastewater treatment methods include separation, sedimentation, coagulation, biological processes, flocculation, and carbon adsorption. Membrane techniques stand out due to their efficiency, speed, cost-effectiveness, integration, and selectivity. Membrane fouling, primarily pore blockage, significantly reduces filtration efficiency and energy requirements. To mitigate this, nanoparticles can be incorporated into or deposited on the membrane, altering its chemical composition. Several modifications (surface functionality, polymer blending, pore size tuning) have already been applied for improving the membrane's efficiency (1, 2, 3). Silica membranes are important in separation processes like gas and liquid filtration, membrane distillation, and chromatography. They have high thermal stability, chemical resistance, and molecular sieving capabilities, which are crucial for efficient and

selective separations. Gold nanoparticles enhance direct contact membrane distillation (DCMD) by reducing fouling, improving hydrophobicity, and enhancing thermal conductivity. This boosts DCMD efficiency for desalination and antibacterial applications (4, 5, 6). Study reveals that during the process of membrane fabrication metal (Cu, Ti, Zn, Fe, Al etc.) could enhance the membrane antifouling, antibacterial and filtration capabilities(1, 7, 8).

Water demand is rising due to urbanization and industry, posing economic challenges. Toxic heavy metals, like Hg, As, Pb, Cr, Ni, Cu, Zn, Fe, Mn and Cd etc., threaten water quality and human health. Nanomaterials are promising candidates for wastewater treatment, offering selective pollutant removal (9, 10, 11). A nanofibrous membrane composed of polyacrylonitrile (PAN) and embedded with gold nanoparticles (Au NPs) was engineered to efficiently separate oil from water and remove dyes from contaminated water. Known as Au@ZIF-8@PAN-TD, this membrane demonstrated remarkable effectiveness in both oil-water separation and catalytic breakdown of organic dyes, such as 4-nitrophenol. With its porous design, it offers a promising solution for the purification of polluted water sources (12, 13, 14, 15).

Doped membranes for direct contact membrane distillation (DCMD) desalination were created by blending hydrophobic macromolecules and hydrophilic polymers. Parameter variations affected performance, with longer evaporation times decreasing flux, and higher contact angles and fluorine content lowering permeate flux. These superior membranes outperformed commercial ones, achieving a 55% higher permeate flux and over 99% NaCl separation. For uniform silica films incorporating stable gold nanoparticles, a controlled sol-gel process was utilized. XPS analysis confirmed stable AuNP properties within the films, displaying altered optical characteristics. SiO_2 nanoparticles increased membrane roughness and contact angle, improving liquid repellency and wetting resistance, achieving nearly 100% salt rejection (16, 17, 18, 19).

This research enhances the global efforts to address water challenges by creating scalable, cost-effective, and eco-friendly Au@SiO_2 membranes. This cutting-edge technology aims to combat water scarcity and bacterial contamination, supporting a safer and more sustainable future for water resources while contributing to the goals of SDG 7 by fostering clean and accessible water solutions. This study innovatively combines gold nanoparticles with SiO_2 membranes, a novel approach not extensively explored in the literature. The comprehensive DFT analysis reveals unique improvements in material properties, leading to superior filtration performance for heavy metals and pathogens, surpassing existing methods.

EXPERIMENTAL WORK

Chemicals

PVP (polyvinylpyrrolidone), butanol, PVA (polyvinyl alcohol), PEG (polyethylene glycol), sodium citrate, ammonia solution (NH_4OH), tetraethyl orthosilicate (TEOS), distilled water, trimethoxyoctylsilane (C_8TMOS), gold chloride ($AuCl_3$). All chemicals were used without further purification.

Fabrication of Gold Doped Silica Membrane

Silica sol. Was prepared by adding 20 µl of Tetraethyl orthosilicate (TEOS – $Si(OC_2H_5)_4$) and 10 µl of Trimethoxyoctylsilane (C_8TMOS) and the mixture is stirred for 15 minutes. After that a separate sol is prepared by combining 6 ml of distilled water with 0.20 g of sodium citrate, followed by the addition of ammonia solution (NH_4OH). This solution is stirred for 15 minutes and then merged with the silica mixture, followed by an additional 15 minutes of stirring. Separately, polyethylene glycol (PEG), polyvinylpyrrolidone (PVP), and polyvinyl alcohol (PVA) are dissolved in butanol, with PVP ($(C_6H_9NO)n$) acting as the precursor. Precisely, 9 g of PVP is dissolved in 8 ml of butanol, and then 30 ml of distilled water is added. This solution is stirred for 30 minutes at a speed of 350-550 rpm. Subsequently, 3 g of PEG and 3 g of PVA are introduced, and the mixture is stirred for an additional 15 minutes. The combined silica sol and other mixtures are incorporated into the polymer solution, and entire mixture is stirred for few minutes. The gold dopant is introduced at this stage in varying

concentrations (5wt%, 10wt%, 15wt% and 20 wt%) at room temperature. Afterward, the mixture is left to rest at room temperature for 24 hours. The synthesized membranes are then dried in an oven at 50°C for 4 hours.

The nutrient agar was dissolved in distilled water to prepare the culture medium, which was then sterilized by autoclaving at 120°C. After sterilization, the medium was poured into petri dishes and left to solidify at room temperature (23°C). Bacterial cultures, including *K. pneumonia* and *S. aureus*, were transferred to agar plates and incubated for 24 hours at 37°C. To create a saline solution, NaCl was dissolved in water, and the resulting solution was inoculated with bacteria. Dilution steps were carefully followed to ensure the preservation of bacterial integrity for use within a 15-minute timeframe (20).

The antibacterial properties of Au@SiO_2 membranes were assessed through the Ager disk diffusion method. Diluted bacterial samples were applied onto agar plates, and sterilized cotton swabs were used to ensure uniform inoculation across all plates. Proper labeling of all plates was done prior to creating the composite sample.

The antibacterial efficacy of Au@SiO_2 membranes was assessed using the agar disc diffusion technique. For the antibacterial tests, *Staphylococcus aureus* (Gram-positive) and *Klebsiella pneumoniae* (Gram-negative) were chosen as the test organisms. The chosen microorganisms were cultured in broth for approximately 24 hours at a concentration of 106 cells/ml and subsequently filtered. Prior to the antibacterial studies, sterilization was carried out using an autoclave. Nutrient agar plates were prepared, sanitized, and solidified. These plates were first treated with 85% methanol and then air-dried within the biosafety cabinet. The membranes, with consistent spacing between each other, were placed onto the agar surface. Membranes containing different concentrations of gold-doped Silica membranes were placed in the incubation chamber and incubated at 37°C for 24 hours before being removed from the incubation chamber.

RESULTS, AND DISCUSSION

FTIR (Fourier Transform Infrared Spectroscopy) for compositional Analysis

Fourier-transform infrared (FTIR) spectra were obtained using an IRTracer-100 spectrometer within the 4000–400 cm^{-1} range. As shown in Figure 1, the resulted spectrum revealed a distinct pike at 1310 cm−1, which is attributed to the asymmetric stretched vibration for Si–Au–Si, confirming the presence of silica materials. Additionally, a pike at 1800 cm−1, related with NH stretching, additional verified that the prepared nanoparticles primarily consisted of silica materials with an amine group. The FTIR spectrum also displayed characteristic bands corresponding to the gold-doped nanoparticles (Table 1). Specifically, peaks at 1495 cm−1, indicative of the C═C deformation vibration, and 2259 cm−1, representing the C–O stretch vibration, were observed. Peaks at 1000 cm−1. (C–N stretching), 841 cm−1 (asymmetric CH2 stretch), 2880 cm−1 (C–H stretch), and 3470 cm−1 (OH stretching) were consistently detected, indicating the presence of gold particles within the membranes. These gold particles influence the molecular vibrations, enhancing the stretching of specific bonds in the composite material and confirming the successful doping of the nanoparticles.

Table 1. Vibrational frequencies (cm^{-1}) and groups in FTIR spectra of gold doped silica membranes (21).

No.	Wavenumber cm^{-1}	Vibrational group
1	3470	OH stretching
2	2880	C-H stretching
3	2259	C-O
4	1800	NH
5	1495	C=C
6	1310	Si-Au-Si
7	1000	C-N
8	841	CH_2 –Asymmetric

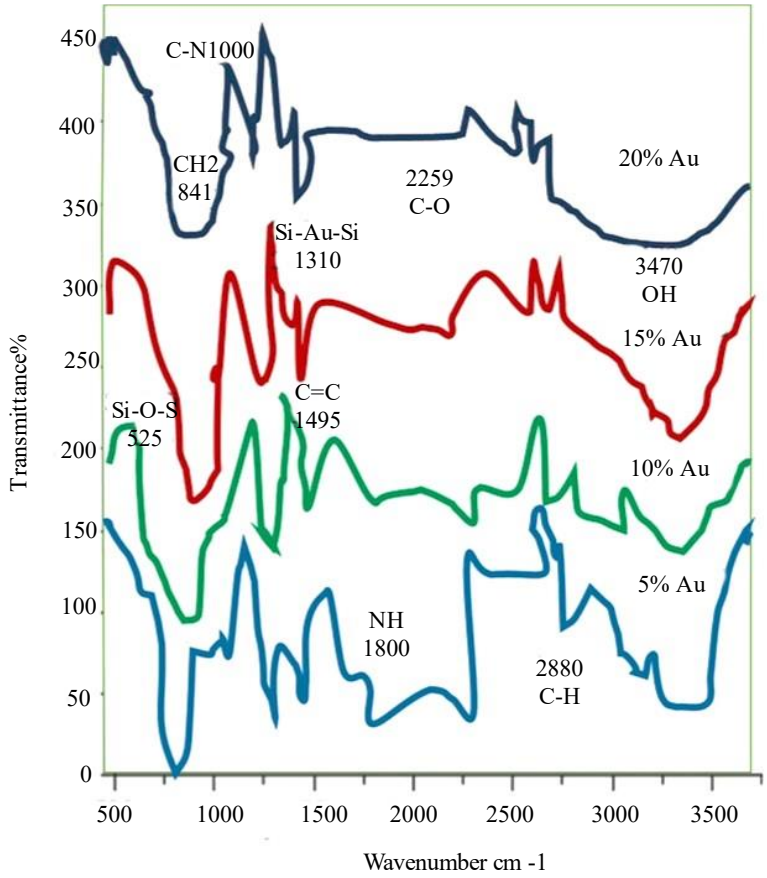

Figure 1. Comparison FTIR spectra of Au 5%, Au 10%, Au 15%, and Au 20% gold doped silica nanoparticles.

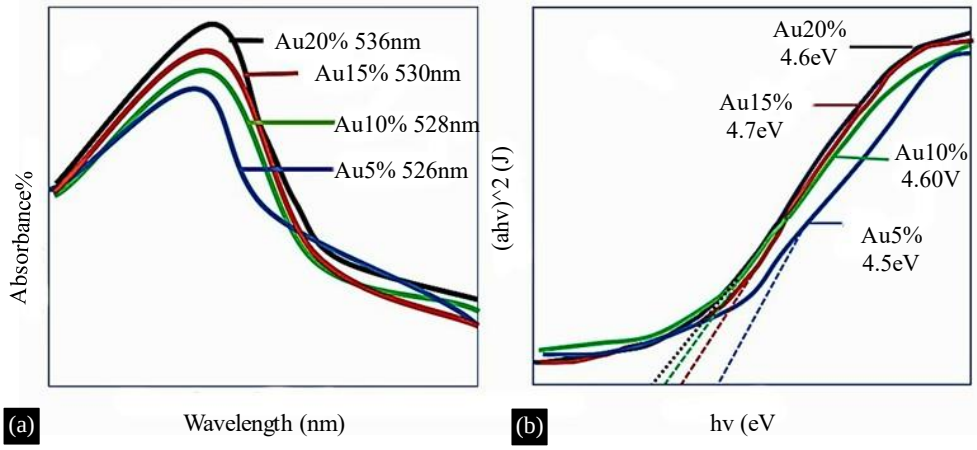

Figure 2. (A) comparison graph of UV-Visible absorption spectra of gold doped silica nanoparticles with different concentration of dopant. (B) comparative band gap of UV-Visible absorption spectra of gold doped silica nanoparticles with different concentrations

UV-Visible Optical Analysis

Optical measurements were conducted by using a U-2800 HITACHI spectrometer, covering a wavelength range from 200-800 nm. The UV/visible resulted spectrum of the fabricated Au@SiO₂ nanoparticles showcased a prominent peak situated around 536 nm (Figure 2(A)). As the gold concentration increases, the absorbance peak undergoes a red shift, meaning it moves to a longer wavelength. It revealed that greater gold content leads to stronger absorbance, indicating more light

absorption. Concurrently, Figure 2 (B) showed that the values of the energy gap (Eg) exhibited a consistent decrease (2.6 eV to 1.8 eV) in correspondence with the incremental elevation of the gold dopant concentration. This observed decline can be attributed to the emergence of structural anomalies within the polymer matrix and an escalated dispersion of the nanoparticles within the membrane (22). The emergence of these structural irregularities stems from the localization of electronic states within the energy bandgap. These localized states lead to overlapping interactions, which in turn reduce the overall energy bandgap. This phenomenon is a consequence of the heightened accumulation of gold dopant content within the membrane matrix.

Morphological and Elemental Analysis

The surface and cross-sectional morphologies of both undoped and Au@SiO_2 membranes were subjected to analysis working on a scanning electron microscope, (SEM) (JEOL: JSM-6480) on an acceleration voltage. of 10 kV. Figures 3(a) to (d) provide a progressive depiction of the top surface of the membrane under varying levels of magnification. As anticipated, in Figure 3(A) (a), the highlighted area showed the undoped membrane on top which demonstrated a uniform and smooth appearance without evident open pores. Conversely, the Au@SiO_2 membranes exhibited an augmented surface roughness as the dopant concentration increased. The SEM images highlighted bright regions denoting the presence of gold particles on the membrane's surface, which were randomly dispersed. In contrast, dark regions indicated the pores of the membranes. An introduction of dopants led to noticeable alterations in the surface structure. At a gold concentration of 5 wt%, distinctive wrinkle structures emerged on the top surface (Figure 3(a)), attributed to turbulence induced by the dopant. Increasing the gold concentration to 10 wt% resulted in the development of porous structures on the previously dense surface (Figure 3(b)). At 15 wt% and 20 wt% concentrations, the initially dense skin layer was completely transformed into a thoroughly rough and porous membrane surface (Figures 3(c) and 3(d)). Notably, at 15 wt%, the silica membranes exhibited multilevel particulate structures (Figure 3(c)), while the top surface predominantly displayed amorphous characteristics. As the gold doping concentration increased to 5%, 10%, 15%, and 20% by weight, the resulting cross-sectional structures remained consistently smooth and porous, as shown in Figures 3(e) through 3(h). Figure 3, with a 5 wt% gold concentration, exhibited a uniform nanostructure, indicating a consistent integration of gold nanoparticles within the silica matrix. Figure 3(f), at 10 wt%, displayed a more intricate and dense morphology, suggesting areas where gold doping may have caused agglomeration or enhanced structural stability. Figure 3(g), with a 15 wt% gold concentration, revealed a porous architecture that is advantageous for applications like water desalination, as it increases surface area and potentially improves filtration efficiency. Figure 3(h), at 20 wt%, demonstrated a highly porous structure with distinct pores distributed throughout the membrane, likely resulting from the higher doping concentration, which could have introduced additional voids or channels within the membrane.

SEM images clearly revealed that gold doping has significantly altered the morphology of the silica membrane. The analysis confirmed a homogeneously distributed pore structure with an average diameter of 40–50 nm, promoting effective water vapor diffusion.

An increase in surface roughness and porosity (as measured by Image J software) can enhance properties like catalytic activity, surface area, and mechanical strength. It could be advantageous for filtration applications, such as in distillation, where greater surface area and controlled porosity are beneficial.

Figure 3(C) the explored the elemental arrangement through Energy Dispersive X-ray (EDX) analysis, aimed at confirming the presence of gold (Au) content. The dispersion pattern of Au within the scrutinized particles concurred within the observed results. Each spectrum distinctly presented the peaks corresponding to Au, in addition to peaks representing elements such as carbon (C), antimony (Sb), nitrogen (N), and oxygen (O), Scandium (Sc), Tellurium (Te), Xenon (Xe), Zinc (Zn), Sodium (Na) etc. These peaks help to identify the main components of the sample, any additional materials present, leftover substances from production, and potential analysis errors.

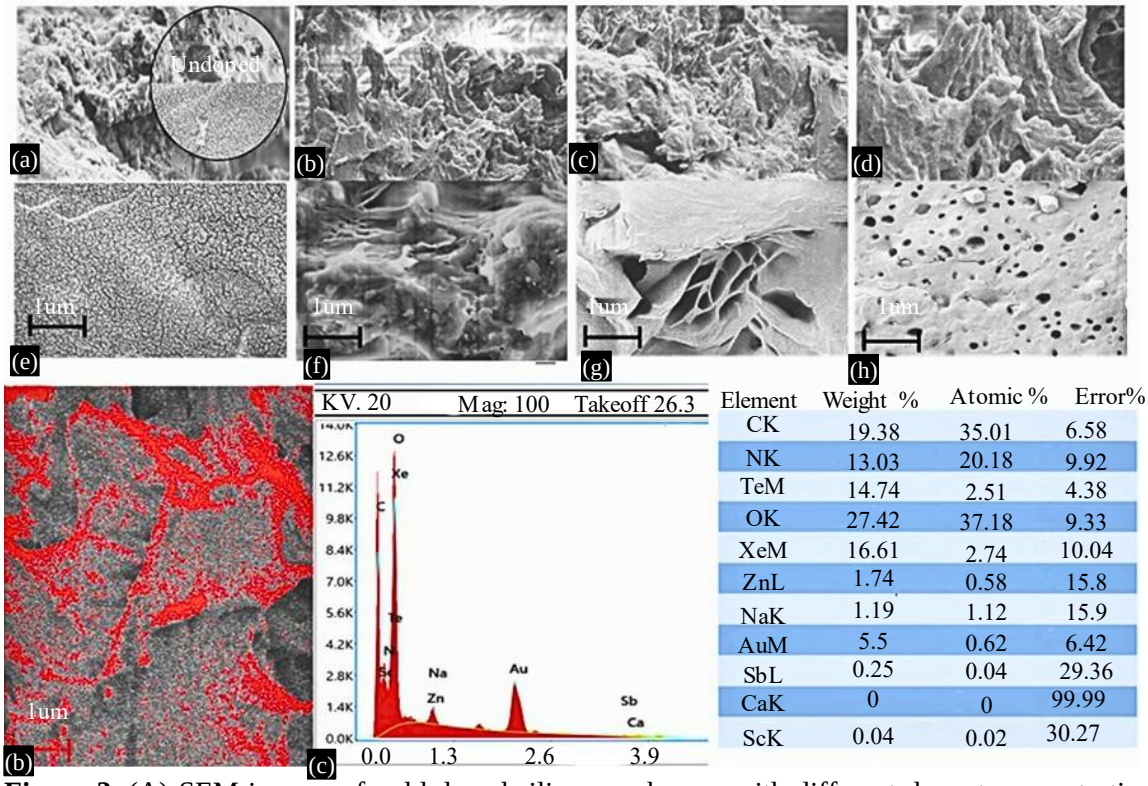

Element	Weight %	Atomic %	Error%
CK	19.38	35.01	6.58
NK	13.03	20.18	9.92
TeM	14.74	2.51	4.38
OK	27.42	37.18	9.33
XeM	16.61	2.74	10.04
ZnL	1.74	0.58	15.8
NaK	1.19	1.12	15.9
AuM	5.5	0.62	6.42
SbL	0.25	0.04	29.36
CaK	0	0	99.99
ScK	0.04	0.02	30.27

Figure 3. (A) SEM images of gold doped silica membranes with different dopant concentrations (a) SEM image of surface for gold 5wt% doping, (b) surface morphology for gold 10wt%, (c) surface morphology for gold 15wt%, (d) surface morphology for gold 20wt%. (e) Cross-sectional SEM image of 5wt% dopant, (f) cross-sectional SEM image for 10wt% dopant, (g) cross-sectional SEM image of 15wt% dopant, (h) cross-section SEM image of 20wt% dopant. (B) Pore size measurement by ImageJ software. (C) EDX plot to show the content of gold dopant in prepared membranes.

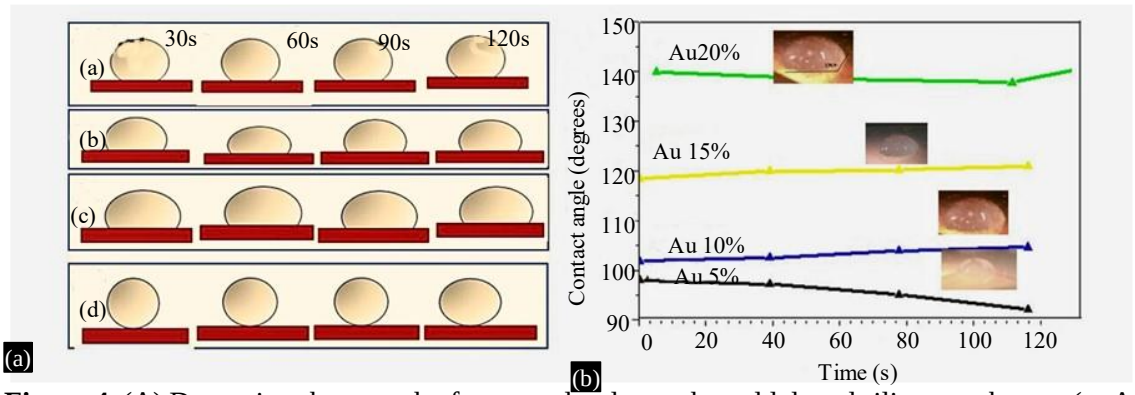

Figure 4. (A) Dynamics photograph of a water droplet on the gold doped silica membranes (a=Au20%, b= Au15%, c=Au10%, d=Au5%) surface at different times from 30 s to 120 s. (B) water contact angle vs time graph of gold doped silica membranes.

Wettability of Prepared Membrane by Contact. Angle

The contact angles of the prepared membranes were determined using a high-resolution digital camera (12 megapixel). The wettability and adhesiveness characteristics of membranes containing Au@SiO₂ were assessed using water contact angle (WCA) measurements under ambient conditions. Upon introducing a 3 μL water droplet onto the surface of the Au-doped silica membrane, an average WCA of 130.9° of was recorded. This significant contact angle persisted for 120 seconds, underscoring the membrane's hydrophobic attributes (depicted in Figure 4a to 4d). Conversely, the initial WCA of the silica membrane stood at 111.8° for Au5%, with the water droplet penetrating the membrane within

a mere 30 seconds (shown in Figure 4(A) (a to d). Remarkably, placement of a water droplet on the Au10%, Au15% and Au20% doped silica membrane led to a heightened WCA of about 145.5°, maintaining this value steadfastly beyond 120 seconds (illustrated in Figure 4(A). This phenomenon was accompanied by the water droplets remaining situated on the surface, exemplifying the Au@SiO_2 membrane's super hydrophobic nature. The water contact angle vs. time graph Figure 4B illustrates the effect of gold doping on the wettability and stability of silica membranes. The membrane's surface hydrophobicity changes over time, indicating dynamic interactions with water. Understanding these variations is vital for enhancing membrane performance in applications such as water desalination.

Direct Contact Membrane Distillation for Water Purification

Membrane distillation (MD). is a thermal process that allows volatile components in vapor form to pass through a hydrophobic membrane. To improve the membrane's resistance to liquid wetting, silica membranes doped with gold nanoparticles. Tests were then showed to compare the performing of the modified membranes with that of the undoped membranes in the presence of sodium dodecyl sulfate. The performance evaluation of gold-doped silica membranes was conducted using a DCMD system featuring three stainless-steel cells. These cells, each with dual chambers (10 cm diameter, 235.6 cm^2 total area), were enclosed by 2.5 to 3 cm compartments with O-rings. Temperature control involved heating the feed chamber and cooling the permeate chamber. The membranes allowed for effective separation. Prior to temperature measurement, steady-state conditions were achieved. Permeate flux was determined by observing water levels in containers for both streams while maintaining equilibrium to prevent water leakage. Flux data points were obtained by averaging three measurements and sometimes using separate sheets for specific membranes (23, 24).

Several DCMD investigations were showed at UGA (University of Georgia, USA) using heavy metal either 0.5 M $PbCl_2$ and Cd $(NO_3)_2.H_2O$ aqueous solution as the feed. The source temperature ranged from 40° to 70°C, while the filtrate temperature remained within 10–15°C for $PbCl_2$ and 65°C was maintained alongside a permeate temperature of 15°C for Cd $(NO_3)_2.H_2O$. The DCMD rejection of heavy metals from Au@ SiO_2 membranes were systematically compared with those of the pure silica membrane displayed in Figure 6B and 6D. DCMD fluxes plotted against the feed inlet temperature, using $PbCl_2$ as the feed (Figure 6(A)) and feed of 0.5 M Cd $(NO_3)_2.H_2O$ (Figure 6(B)). Evidently, both the unadulterated silica membrane and the Au@SiO_2 membranes demonstrate an exponential augmentation in DCMD flux with the escalation of the feed inlet temperature. A consistent trend emerges from both figures, showcasing the flux order as

Au20wt% > Au15wt% > Au10wt% > Au5wt% > pure.

Comparatively, the prepared doped membranes exhibited an elevated permeate fluxes in comparison to the silica membrane. Among the different doping concentrations, the 20 wt% Au@SiO_2 membrane (Au20wt%) exhibited the most superior performance for DCMD applications. Particularly noteworthy, the DCMD flux of the Au4 membrane surpassed that of the pure silica membrane by an impressive 65%. When considering the utilization of a Cd $(NO_3)_2.H_2O$ aqueous solution as the feed, the obtained permeate flux was found to be 25–30% lower in comparison to the flux obtained using $PbCl_2$ as the feed. This discrepancy is attributed to the diminished vapor pressure of the salt solution. Furthermore, a decline in the DCMD flux can be attributed to concentration polarization arising from the presence of the Cd $(NO_3)_2.H_2O$ solute on the source side of the prepared membrane.

$$A = (1- Cp/Cf)\ 100$$

Where, Cp and Cf are the feed meditation in filtrate and bulk feed, respectively. In reference to experiments involving the heavy metal solution, the solute division factor, denoted by α, was consistently calculated above 99% for all five membranes tested. This indicated the efficacy of the gold-doped membranes (Au5wt%, Au10wt%, Au15wt%, and Au20wt%) as potential MD membranes, aligning with prior research (25, 26). Conversely, Figure 6(B) and (D) showed that the Au0wt% membrane displayed an inability to reject metals. So, we concluded that the incorporation of gold nanoparticles in silica membranes not only improved their hydrophobicity but also enhanced their heavy metal rejection capabilities, making them promising candidates for desalination and water purification processes.

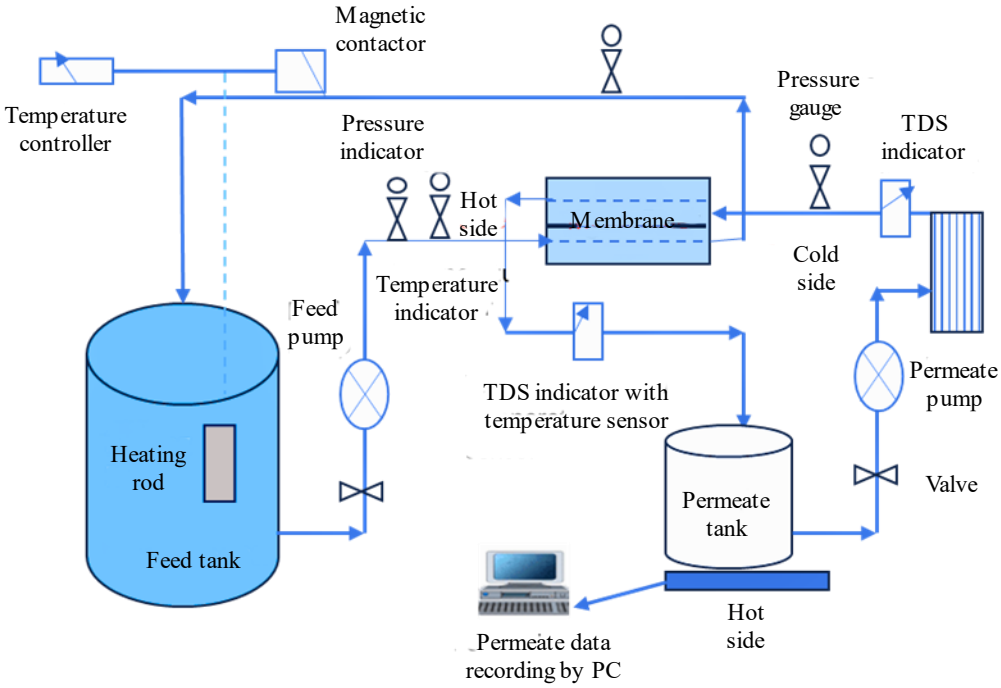

Figure 5. Schematic diagram of direct contact membrane distillation (20).

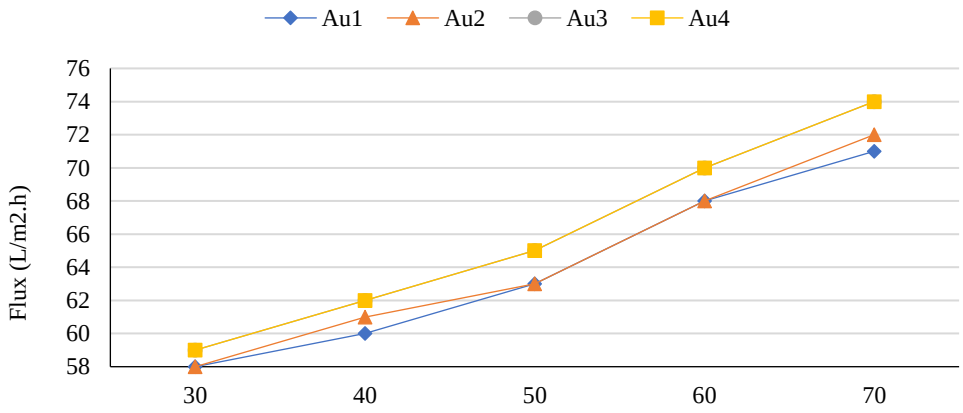

(a)

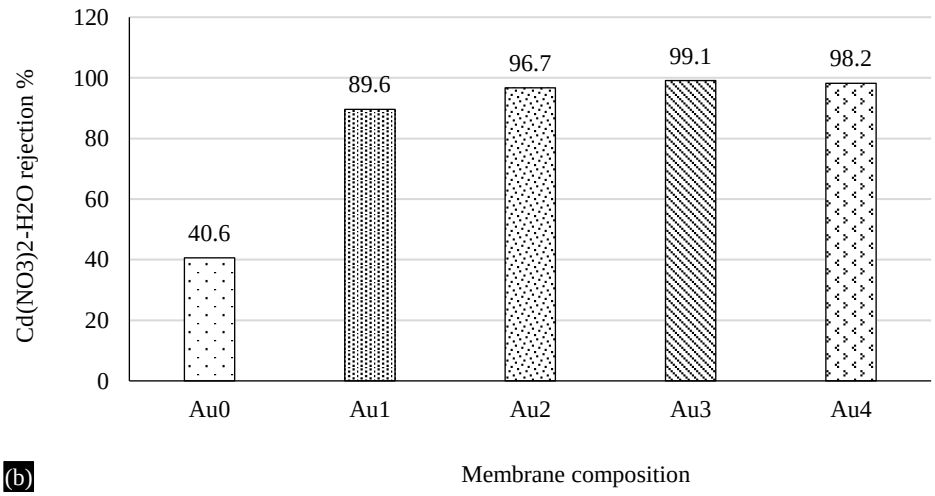

(b)

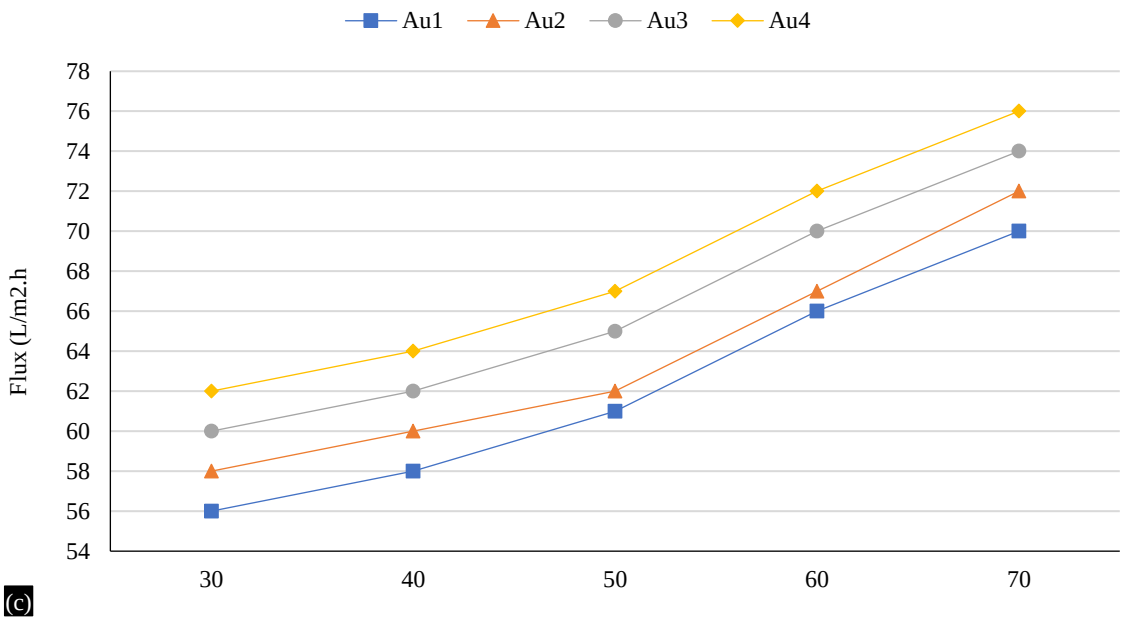

(c)

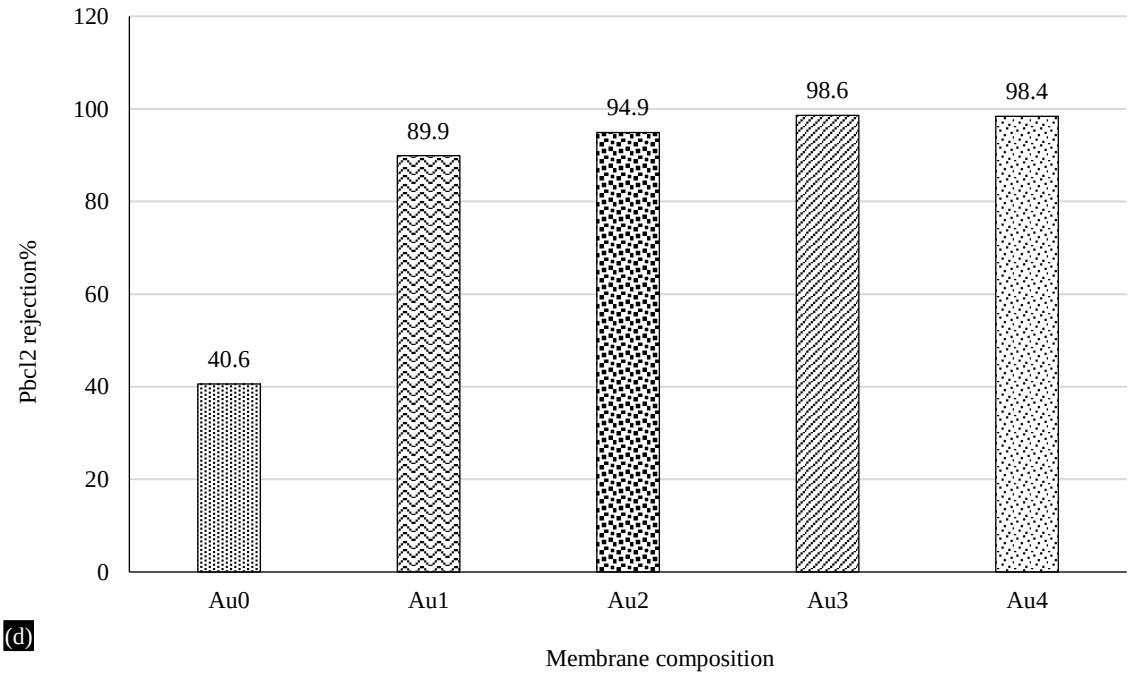

(d)

Figure 6. Membrane performance with the effect of solvent type and heavy metal rejection. (A) source temperature consequence on flux of $PbCl_2$ as feed solution. (B) Membrane composition VS $PbCl_2$ heavy metal rejection, (C) source temperature consequence on flux of Cd $(NO_3)_2.H_2O$ water as feed solution. (D) Membrane composition VS Cd $(NO_3)_2.H_2O$ heavy metal rejection.

Anti-Bacterial Activity of Gold Doped Silica Membrane

Figure 7 (A and B) revealed that all synthetic membranes exhibited the antibacterial effects against *S. aureus* and *K. pneumoniae* bacterial strains. Both undoped and Au@SiO_2 membranes show a similar zone of inhibition (ZOI) of 33mm against S. Aureus (Figure 7(C)). Notably, as the level of Au doping rises, there is a obvious slowdown re-growth before it eventually disappears. This change in antibacterial activity with metal doping might be attributed to alterations in particle size and shape, which may enhance the silica's antibacterial properties.

In the case of *K. pneumoniae*, the ZOI diminishes for undoped silica membrane and increases with the increase in gold doping. This difference in antibacterial activity between Au-doped silica membranes in contrast to Gram-negative and Gram-positive bacterial strains could be due to variations in bacterial species' cell wall strength or membrane composition.

Analysis of Density Field in Gold-Doped Silica Membranes by Forcite Module

To understand the impact of Au@SiO_2 membranes on water desalination performance, the density field of Au@SiO_2 membranes was examined. As revealed in Figure 8(A) gold nanoparticles (red spheres) were embedded within the silica matrix (yellow spheres). The membrane's structural and functional properties were significantly affected by the density and distribution of these nanoparticles.

The factors which are essential for water desalination were studied by DFT as follows:

1. *Dispersion and uniformity*: The dispersion of gold nanoparticles within the silica matrix appears dense and largely uniform as shown in Figure 8(A). This uniformity is crucial for maintaining consistent membrane performance across its entire surface. Variations in distribution can lead to localized differences in permeability and selectivity, potentially affecting the overall desalination efficiency (27, 28).
2. *Particle size and density:* The size and density of the gold nanoparticles are crucial for the membrane's efficiency. Smaller, denser gold particles create a larger surface area for interacting with water molecules. This increased surface area enhances the catalytic activity, which can improve the breakdown and removal of contaminants during desalination (29).

Figure (8B and 8C) showed that DFT analysis reveals the impact of particle size and density on material stability, showing a trend of decreasing geometry optimization parameters (bond lengths, angles, and atomic positions). As optimization progresses, total energy, atomic forces, and stress levels typically decrease, indicating a shift toward a more stable configuration. Comparative density field graphs, displayed the variations in particle size, overall density distribution and structural properties. This declining trend in geometry optimization underscores the importance of precise control over particle dispersion and arrangement to achieve optimal material performance.

Radius of Gyration vs. Parameter

The graph (Figure 8D) illustrates the relationship between the radius of gyration and the parameter (expressed in inverse Angstroms).

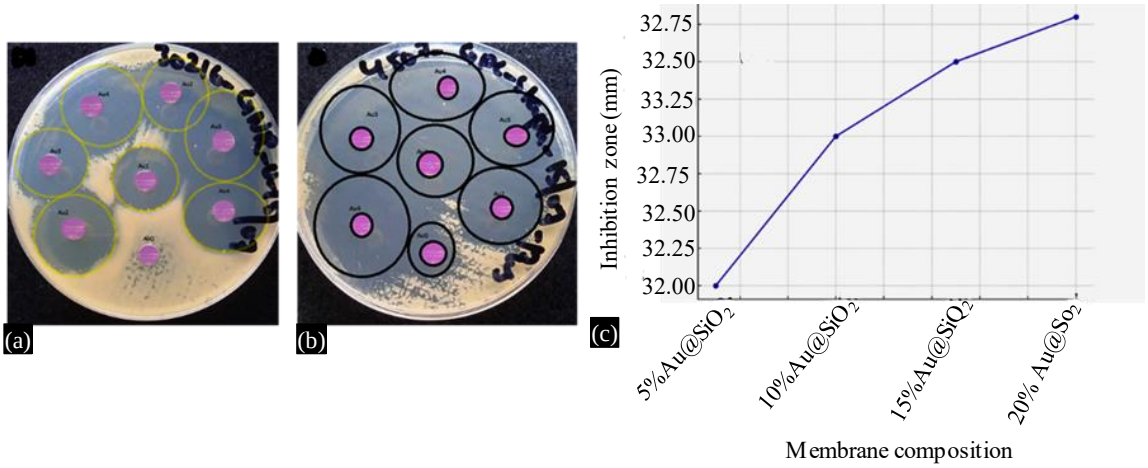

Figure 7. The outcome following 24 hours of incubation at 37°C showed the existence of an inhibition zone in both undoped silica membranes and gold doped silica membranes when in contact with two types of bacteria: a) *K. pneumonia* and b) *S.auers*. (C) Membrane composition against inhibition zone showed that with the increase in gold doping inhibition zone slightly increases.

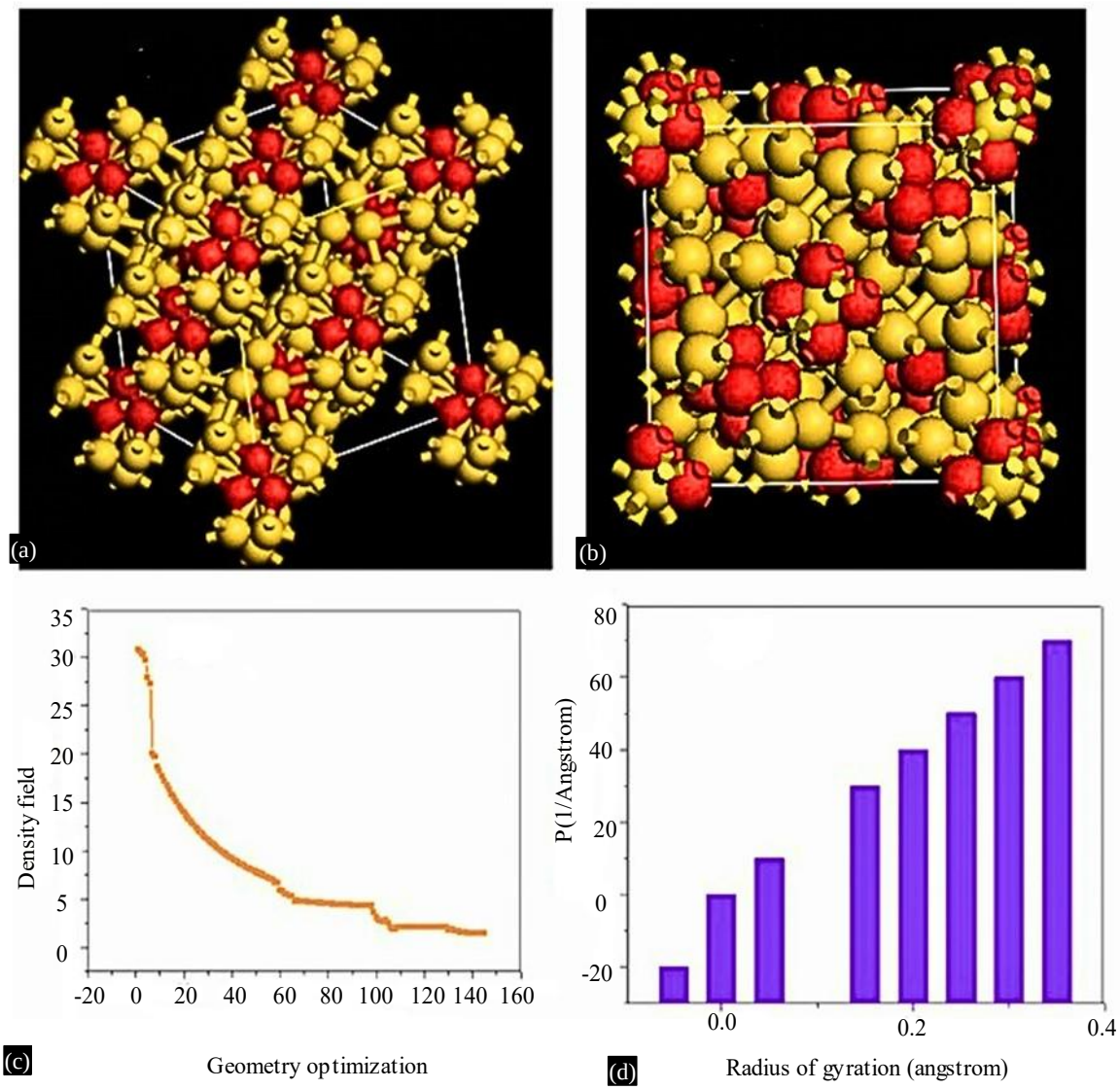

Figure 8. (A) Gold doped silica membranes density functional theory structure. (B) DFT analysis of particle size and density and (C) geometry optimization versus density field graph. (D) Relationship of radius of gyration and Perimeter (P).

Radius of gyration (x-axis): This metric indicates the dispersion of gold nanoparticles within the silica matrix relative to a central point.

Parimeter (P) (y-axis): characterizes the density field and structural arrangement of the nanoparticles.

Upward trend: The graph showed that as the radius of gyration rises, the parameter likewise rises. This proposes that as the nanoparticles become more dispersed the value of perimeter (P) increases. This trend indicates a correlation between greater nanoparticle dispersion and an increase in the structural characteristic represented by (P).

This confirms the wide distribution of gold nanoparticles within the silica matrix. A higher dispersion can enhance interactions with water molecules, potentially increasing the effective surface area, which exhibit better permeability and selectivity (30). This is supported by the correlation between larger radii of gyration and higher P values, which are crucial for effective desalination by allowing better water flow while selectively rejecting unwanted ions.

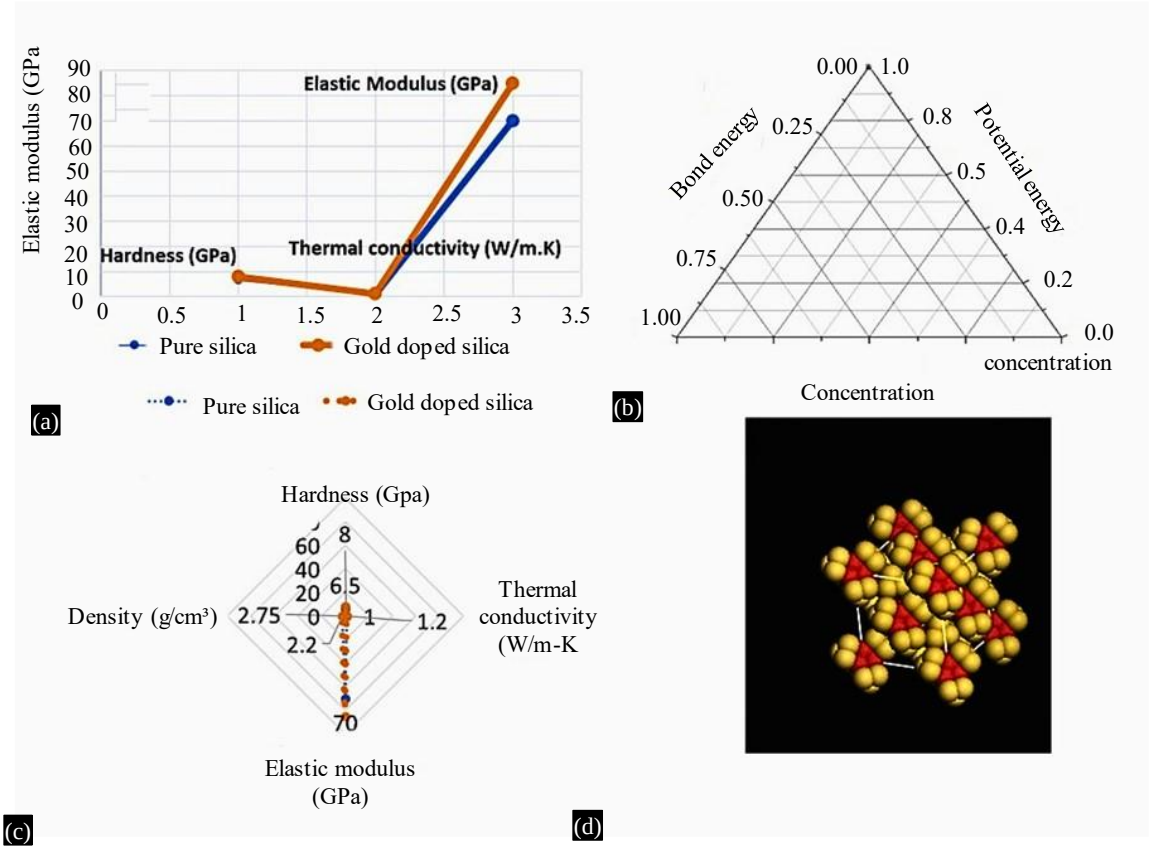

Figure 9. (A) The comparison graph shows that elastic modulus, thermal conductivity and hardness is increasing with gold doping. (B) Relation between bond energy, potential energy and concentration of gold doping. (C) Illustration shows the relation between density, hardness, thermal conductivity and elastic modulus. (D) Pictorial representation of density and pore size.

Elastic modulus, thermal conductivity and hardness: The mechanical strength of the Au@SiO₂ membranes increased by 21%, with the elastic modulus rising from 70 GPa in pure silica to 85 GPa in the gold-doped membranes shown in Figure 9A. Hardness measurements also showed an increase from 6.5 GPa to 8.0 GPa. The thermal conductivity of the Au@SiO₂ membranes was measured at 1.2 W/m·K, indicating a 20% enhancement compared to 1.0 W/m·K for pure silica by using Forcite module.

The Ternary Plot for Gold-Doped Silica Membranes

The ternary plot illustrates (Figure 9(B)) the balance between Bond Energy, Potential Energy, and Concentration in gold-doped silica membranes. Stronger energy bonds between silica and gold lead to increase the membrane stability. The arrangement of nanoparticles stores energy, impacting the membrane's structure. The bond energy of gold nanoparticles enhances the membrane's optical properties, antibacterial effectiveness, and desalination performance.

Density of gold-doped silica membranes: The Au@SiO₂ membranes exhibited a density of 2.75 g/cm³, which represents a 25% increase compared to the density of pure silica. This increase is attributed to the higher atomic mass of gold. Figure 9C depicted that simulation results indicate that the gold doping does not induce significant structural distortions in the silica framework. The distribution of gold atoms within the membrane appears uniform, with no adverse effects on the overall structure. The Figure 9C showed that the combination of gold atoms into the silica matrix introduces new electronic states within the silica band gap. This modification may enhance optical properties, such as light absorption or scattering, which could benefit light-assisted desalination techniques. Figure 9D showed that by adding gold to the silica matrix alters the membrane's porosity and pore size distribution. Gold

nanoparticles can create more refined pore structures, which are essential for selective ion rejection. A well-distributed pore size improves water permeability while maintaining high selectivity, both of which are vital for effective desalination (28). The introduction of gold into the membranes may enhance their resistance to mechanical stress, as evidenced by the increase in elastic modulus. However, changes in thermal conductivity could influence the membrane's thermal regulation during operation. Achieving an optimal balance between these factors is crucial for enhancing membrane performance in practical applications(31).

CONCLUSION

This study provides a comprehensive assessment of gold-doped silica ($Au@SiO_2$) membranes, emphasizing their potential in advanced water desalination and antibacterial applications. By employing sol-gel techniques, gold nanoparticles were successfully incorporated into the silica matrix, with the resulting membranes characterized through several analytical methods. Structural analysis via Scanning Electron Microscopy (SEM) revealed a well-distributed pore structure with an average pore size of 40-50 nm, ensuring effective water vapor transport. Fourier Transform Infrared Spectroscopy (FTIR) identified key bonding features, including Si-O-Si and Si-Au-Si peaks at 525 cm^{-1}, and 1310 cm^{-1} respectively, confirming the successful integration of gold nanoparticles. Energy-Dispersive X-ray Spectroscopy (EDX) quantified the gold content at 1.5 wt%, and UV-Visible spectroscopy demonstrated a notable decrease in the optical energy gap from 2.6 eV down to 1.8 eV, indicating enhanced electronic properties. The membranes exhibited a water vapor transport rate of 3.2 kg/m^2h, reflecting efficient permeation performance. Additionally, they achieved remarkable heavy metal rejection rates, exceeding 99.5% for both Pb^{2+} and Cd^{2+}, underscoring their effectiveness in removing toxic contaminants from water. Antibacterial assays confirmed that these membranes significantly reduce bacterial colonies, achieving a 98% reduction for *Kleb pneumoniae* and a 96% reduction for *Staphylococcus aureus*. These results highlighted the membranes' robust antimicrobial properties. Density Functional Theory (DFT) calculations demonstrated that gold doping resulted in a 1.2 eV reduction in the band gap, a 15% drop in total stress, improvements in both elastic modulus and thermal conductivity, along with a 20% rise in bond energy and an 18% increase in potential energy. Experimental data corroborated these findings, revealing that the large ionic radius of gold limits its full incorporation into the silica matrix and contributed to the observed structural modifications. The gold-doped silica membranes demonstrated significant advancements in both water purification and antibacterial performance. Their high efficiency in water purification and remarkable ability to inhibit microbial growth highlight their potential as versatile and effective solutions for modern water treatment challenges.

POTENTIAL APPLICATIONS AND FUTURE WORK

The gold-doped silica membranes demonstrated promising attributes for desalination purposes. Further experimental validation and optimization of doping levels could improve their performance. Additionally, exploring the interplay between mechanical, electrical, and thermal properties may lead to the development of more durable and efficient membrane designs.

REFERENCES

1. Damiri F, Andra, S., Kommineni, N., Balu, S. K., Bulusu, R., Boseila, A. A., ... & Cavalu, S. . Recent advances in adsorptive nanocomposite membranes for heavy metals ion removal from contaminated water: A comprehensive review. . Materials,. 2022; 15(15), :5392.
2. Govindarajan PR, Shanmugavel, R., Palanisamy, S., Khan, T., & Ahmed, O. S. Crash-worthiness analysis of hollow hybrid structural tube by aluminum with basalt-bamboo hybrid fiber laminates by roll wrapping method. . BioResources, . 2024;19(2), :3106.
3. Mubarak S, Byun, H. S., Dhamodharan, D., Divakaran, N., Kumar, P. A., Siddique, A. B., ... & Palanisamy, S. Functionalized black phosphorous-based polymer nanocomposites. . In Advances in Functionalized Polymer Nanocomposites. 2024:307-37.

4. Elma M, Yacou, C., Wang, D. K., Smart, S., & da Costa, J. C. D. . Microporous silica-based membranes for desalination. Water. 2012;4(3):629-49.
5. Emam HE. Accessibility of green synthesized nanopalladium in water treatment,. Results in Engineering. 2022;15:100500.
6. Qtaishat M, Rana, D., Khayet, M., & Matsuura, T. Preparation and characterization of novel hydrophobic/hydrophilic polyetherimide composite membranes for desalination by direct contact membrane distillation. . Journal of Membrane Science, . 2009;327(1-2), :264-73.
7. Praveen Kumar M, Mangalaraja, R. V., Karazhanov, S., de Oliveira, T. F., Sasikumar, M., Murugadoss, G., ... & Kumaresan, N. An overview of noble-metal-free nanostructured electrocatalysts for overall water splitting. Materials Technology for the Energy and Environmental Nexus. 2023;1:3-1.
8. Alex Y, Divakaran, N., Kumar, P. A., Dhamodharan, D., Mubarak, S., Wang, J., ... & Srinivasan, P. Computational studies and modeling aspects of functionalized polymer nanocomposites. . Advances in Functionalized Polymer Nanocomposites, . 2024:1001-30.
9. Jiang Y, Jenjob, R., & Yang, S. G. . Enhanced therapeutic potential of irreversible electroporation under combination with gold-doped mesoporous silica nanoparticles against EMT-6 breast cancer cells. . Biosensors, . 2022;13(1), :41. .
10. C. Shang LW, J. Xia, S. Zhang, . Macropatterning of microcrumpled nanofiltration membranes by spacer imprinting for low-scaling desalination, . Environ Sci Technol. 2020;54:15527–33.
11. Zhang Y, Chong, J. Y., Xu, R., & Wang, R. Effective separation of water-DMSO through solvent resistant membrane distillation (SR-MD). . Water Research,. 2021; 197, :117103.
12. Ismail N, Venault, A., Mikkola, J. P., Bouyer, D., Drioli, E., & Kiadeh, N. T. H. . Investigating the potential of membranes formed by the vapor induced phase separation process. . Journal of Membrane Science, . 2020;597, :117601. .
13. Lu KJ, Zhao, D., Chen, Y., Chang, J., & Chung, T. S. . Rheologically controlled design of nature-inspired superhydrophobic and self-cleaning membranes for clean water production. . npj Clean Water, . 2020;3(1), :30. .
14. Kumar P, Mathpal, M. C., Ghosh, S., Inwati, G. K., Maze, J. R., Duvenhage, M. M., ... & Swart, H. C. . Plasmonic Au nanoparticles embedded in glass: Study of TOF-SIMS, XPS and its enhanced antimicrobial activities. . Journal of Alloys and Compounds, . 2022;909,:164789.
15. Mageshwaran V, Sivasubramanian, P., Kumar, P., & Nagaraju, Y. . Antibacterial response of nanostructured chitosan hybrid materials. Chitosan Nanocomposites:. Bionanomechanical Applications,. 2023:161-79.
16. Lu KJ, Liang, C. Z., Chen, Y., & Chung, T. S. Unlock the secret of air blowing in developing high strength and superhydrophobic membranes for membrane distillation. Desalination, . 2022;527, :115579. .
17. Zhang Z, Yang, Y., Li, C., & Liu, R. . Porous nanofibrous superhydrophobic membrane with embedded Au nanoparticles for the integration of oil/water separation and catalytic degradation. . Journal of Membrane Science, . 2019;582, :350-7. .
18. Tian H, Hong, J., Li, C., Qiu, Y., Li, M., Qin, Z., ... & Yin, X. . Electrospinning membranes with Au@ carbon dots: Low toxicity and efficient antibacterial photothermal therapy. . Biomaterials Advances, . 2022;142, :213155. .
19. Liu L, Xiao, Z., Liu, Y., Li, X., Yin, H., Volkov, A., & He, T. . Understanding the fouling/scaling resistance of superhydrophobic/omniphobic membranes in membrane distillation. Desalination, . 2021;499, :114864.
20. Al-Furaiji M, Arena, J. T., Ren, J., Benes, N., Nijmeijer, A., & McCutcheon, J. R. . Triple-layer nanofiber membranes for treating high salinity brines using direct contact membrane distillation. Membranes, . 2019;9(5), :60. .
21. Kekeç S, Kürkçüoğlu, G. S., Yeşilel, O. Z., & Şahin, O. Syntheses, crystal structures, spectroscopic and thermal properties of 3D heteronuclear coordination polymers with 4-ethylpyridine and cyanide ligands. . Structural Chemistry,. 2024; 35(4), :1075-83.

22. Alizadeh M, Dorranian, D., & Sari, A. H. . Comparison of the antimicrobial photocatalytic activities of SiO2 and Au@ SiO2 nanostructures in water decontamination. . Microscopy Research and Technique, . 2024;87(5), :896-907.
23. Ravi J, Othman, M. H. D., Matsuura, T., Bilad, M. R. I., El-Badawy, T. H., Aziz, F., ... & Jaafar, J. . Polymeric membranes for desalination using membrane distillation: A review. . Desalination, . 2020;490, :114530. .
24. Zunita M, Makertihartha, I. G. B. N., Saputra, F. A., Syaifi, Y. S., & Wenten, I. G. . Metal oxide based antibacterial membrane, In IOP Conference Series:. Materials Science and Engineering2018. p. 012021.
25. Ielo I, Giacobello, F., Castellano, A., Sfameni, S., Rando, G., & Plutino, M. R. Development of antibacterial and antifouling innovative and eco-sustainable sol–gel based materials: From marine areas protection to healthcare applications. . Gels, . 2021;8(1), :26.
26. Son HY, Kim, K. R., Lee, J. B., Le Kim, T. H., Jang, J., Kim, S. J., ... & Nam, Y. S. . Bioinspired synthesis of mesoporous gold-silica hybrid microspheres as recyclable colloidal SERS substrates. . 2017.
27. Cho HS, Noh, M. S., Kim, Y. H., Namgung, J., Yoo, K., Shin, M. S., ... & Jun, B. H. . Recent Studies on Metal-Embedded Silica Nanoparticles for Biological Applications. . Nanomaterials, . 2024;14(3),: 268.
28. Darling SB. Perspective: Interfacial materials at the interface of energy and water. . Journal of Applied Physics, . 2018;124(3).
29. Karanovic D, Hadnadjev-Kostic, M., Vulic, T., Markov, S., Tomic, A., Miljevic, B., & Rajakovic-Ognjanovic, V. Thermal treatment impact on the evolution of active phases in layered double hydroxide-based ZnCr photocatalysts: Photodegradation and antibacterial performance. . Green Processing and Synthesis, . 2024;13(1), :20230269.
30. Jelmy EJ, Thomas, N., Mathew, D. T., Louis, J., Padmanabhan, N. T., Kumaravel, V., ... & Pillai, S. C. . Impact of structure, doping and defect-engineering in 2D materials on CO 2 capture and conversion. Reaction Chemistry & Engineering,. 2021; 6(10), :1701-38. .
31. Li C, Dong, H., & Cheng, B. . Tip vortices formation and evolution of rotating wings at low Reynolds numbers. . Physics of Fluids,. 2020; 32(2).

